

Article

Fossilized Bacteria in Fe-Mn-Mineralization: Evidence from the Legrena Valley, W. Lavrion Mine (Greece)

Charalampos Vasilatos *  and Maria Economou-Eliopoulos

Department of Geology and Geoenvironment, National and Kapodistrian University of Athens, 15784 Athens, Greece; econom@geol.uoa.gr

* Correspondence: vasilatos@geol.uoa.gr; Tel.: +30-6976-556-762

Received: 17 December 2017; Accepted: 6 March 2018; Published: 8 March 2018

Abstract: The primary mineralization in the famous Lavrion mine in the Lavreotiki area, Attica (Greece), associated with a granodiorite intrusion of Upper Miocene age and composed of massive sulphide Pb-Zn-Ag ores [sphalerite, pyrite and galena (B.P.G)], has been extensively studied. The present study is focused on thin, hard, dark brown to black Fe-Mn crusts (a few mm to cm in thickness) in the Legrena valley, SW Lavreotiki, aiming to provide new insights on that type of Fe-Mn-mineralization. The scanning electron microscope (SEM)/energy dispersive spectroscopy (EDS) data presented revealed the presence of fine rounded fragments, resembling nodules (up to 200 μm) and fossilized bacteriomorphic Fe-Mn-oxides/hydroxides, within brecciated and foliated zones of carbonate rocks. They exhibit unusual features when compared to the common massive Fe-Mn mineralization with regards the following: (a) the extensive occurrence of bacteriomorphic Fe-oxides/hydroxides and their micro-textures; and (b) the minor elements (K, Na, P, S, Ca, As and Cl). The occurrence of abundant bacteriomorphic Fe-Mn-oxides/hydroxides in the samples from the Legrena valley may reflect their catalytic role in the redox reactions during ore-forming processes. The characteristic features of that type of Fe-Mn mineralization seems to be the result of multistage supergene processes superimposed over initial hydrothermal stages. Such a multistage remobilization and precipitation of metals along open space surfaces on karstified carbonates during a subsequent stage of their initial precipitation may be widespread in the Attica region, Greece.

Keywords: Fe-Mn-mineralization; Legrena valley; Lavrion; fossilized bacteria; microorganisms

1. Introduction

The famous Lavrion mine in Attica (Greece) is well known for the production of silver, since ancient times (earlier than 1000 B.C.). It represents a major Carbonate Replacement Deposit (CRD), associated with a granodiorite intrusion of Upper Miocene age [1]. The primary ore, composed of massive sulphides of sphalerite, pyrite and galena (B.P.G), has been studied by many authors [1–7]. Near a detachment horizon, hydrothermal fluids originating from Miocene intrusions led to high-temperature carbonate stratabound Pb-Ag-Zn ore deposits. Carbon- and O-isotope analyses of the carbonate host have suggested high water-to-rock ratios during brittle deformation, and that water-rock interaction has played the dominant role in the mineralization.

Fe-Mn mineralization throughout Lavreotiki area, Lavrion, extending to NE Attica is commonly hosted within carbonate rocks, close to the contact with the detachment faults between lower and upper marbles and with the Kessariani schists [1,5,8–11] (Figure 1). Although the Fe-Mn-mineralization is widespread along the detachment zones in the Attic-Cycladic belt (including Attica), it exhibits a complex mineralogical and chemical composition and more research is required for better understanding the genesis of that type of mineralization [1,5,7,10–12].

The occurrence of small (a few mm to some cm, in thickness) hard dark brown-black crusts of Fe-Mn-oxides/hydroxides at the Legrena valley, imply their formation during a subsequent stage of their initial deposition. In addition, the association of microorganism in that type of Fe-Mn mineralization, may suggest a controlling role on the creation of the appropriate conditions for Fe/Mn redox reactions, and hence metal bio-leaching and bio-mineralization [8,9].

In the present study, scanning electron microscope (SEM)/energy dispersive spectroscopy (EDS) data revealed—for the first time—the presence of small nodule-like texture forms and fossilized bacteriomorphic Fe-Mn-oxides/hydroxides. We present these data, along with bulk ore major and trace elements composition, aiming to provide new insights into this type of Fe-Mn-mineralization.

2. Geological Outline

The Lavrion district (Figure 1) belongs to the Attic-Cycladic Crystalline Belt, which represents a multistage metamorphic region that includes two major geological units, the lower tectonic unit (LTU) and the upper tectonic unit (UTU) [13,14]. In that area, the LTU consists of an autochthonous sequence of Triassic-Lower Jurassic rocks, metamorphosed from greenschist to amphibolite. That includes the Lower marble series, the Kessariani schists and the Upper marble series, which are all overlain transgressively by non-metamorphic conglomerates and limestones of Upper Jurassic-Lower Cretaceous age [1,14]. The LTU was overthrust by a blueschist facies phyllitic nappe (allochthonous sequence or Intermediate Tectonic Unit) of a probable Upper Cretaceous age [1,13,14]. The Lavrion granodioritic intrusions were synchronous, with the Miocene extensional detachment faulting as a part of a metamorphic core complex formation in the Attic-Cycladic Crystalline Belt [15–19].

In general, mineralization in the Attic-Cycladic Crystalline Belt is associated with successive stages of tectono-plutonic evolution and is closely related to the extensional faulting [20]. Ascending hydrothermal fluids deposited massive sulfide ore in carbonate rocks, while skarn-type mineralization is associated with contact metamorphism around granitoid intrusions [1,4–7,21]. Late NW–SE-trending tension gashes have acted as conduits for ascending hydrothermal fluid, resulting in the formation of mineralized veins [5,6].

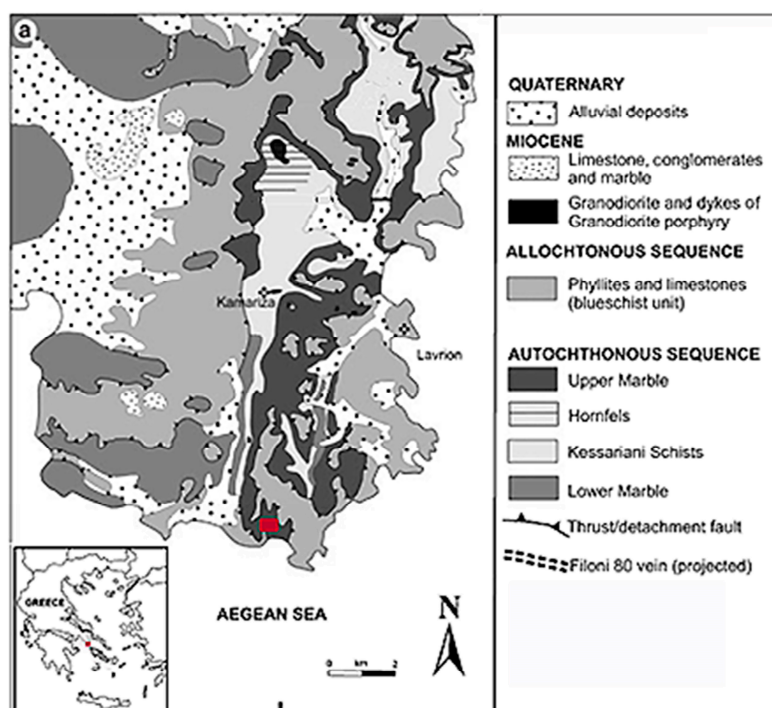


Figure 1. Simplified geological map of the Lavrion ore district (modified after [1,6,22]), showing the location of the studied Fe-Mn-mineralization (red rectangle).

Fe-Mn mineralization at western Lavrion is commonly hosted within carbonate rocks, close to the surface of the detachment faults, and the contacts between lower and upper marbles with the Kessariani schist [1]. Typical iron-rich gossan formation, located at and close to the surface of the detachment fault, such as at the areas of Elafo and Thorikos, has been interpreted to be formed during supergene processes by downward-penetrating water, oxidation of hypogene sulphide mineralization, mobilization of metals and re-precipitation, as a result of the interaction of acidic water with marble [5].

At the Legrena valley (Figure 1), Fe-Mn-crusts of dark brown to black color cover Fe-Mn-ore that is hosted within open space in brecciated and foliated zones of carbonate rocks. They are composed of unusually small (few mm in thickness), hard rounded fragments, cemented by Mn-Fe-material, consisting mostly of bacteriomorphic Mn-Fe hydroxides and pyrolusite (Figures 2–5).

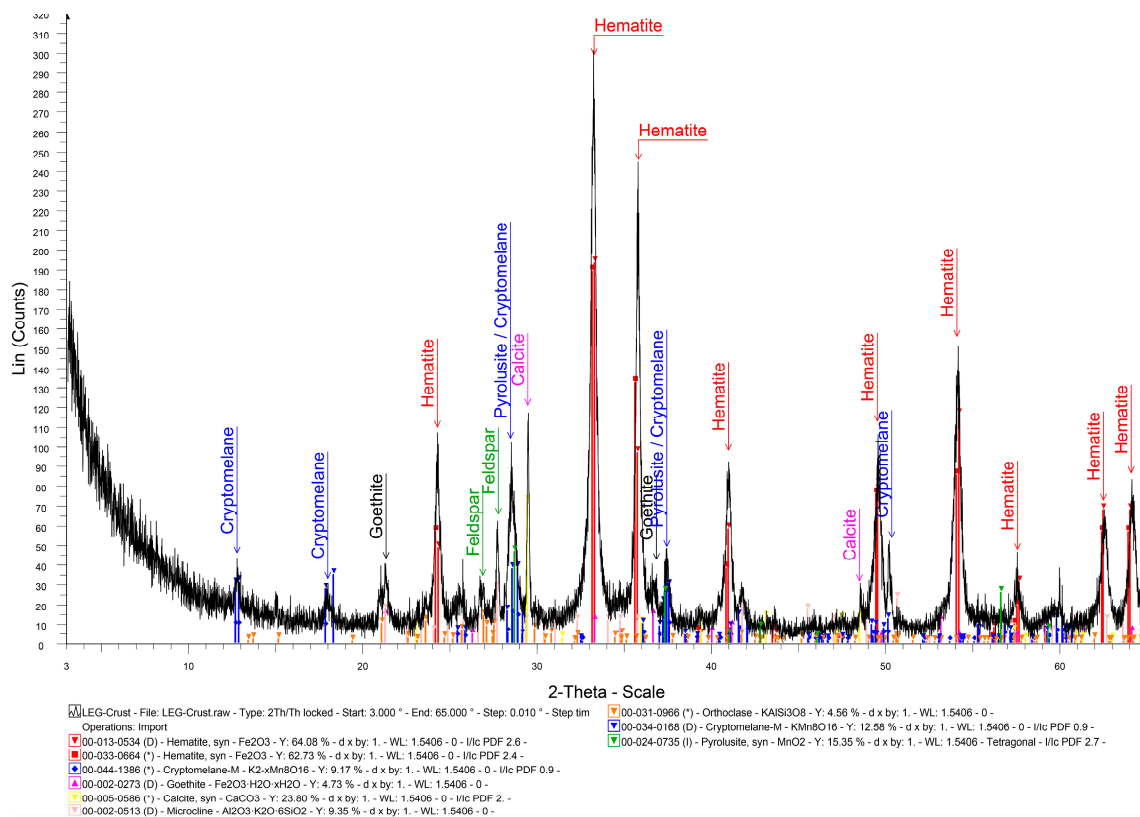


Figure 2. X-ray powder diffraction (XRD) pattern of a Fe-Mn crust sample from the Legrena valley, Lavrion. The high background, the low intensity (number of counts) and the broad peak shape suggest a low grade crystallinity of the major mineral phases.

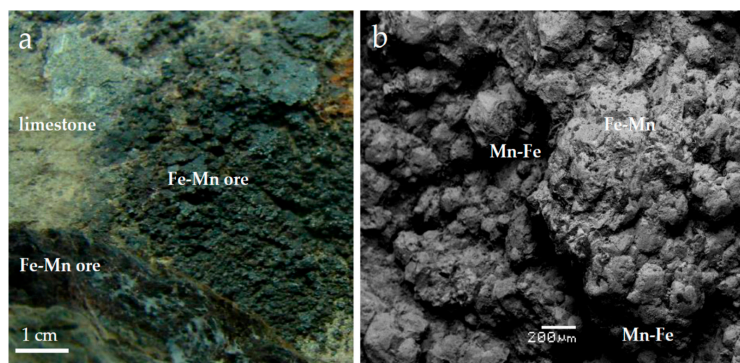


Figure 3. Cont.

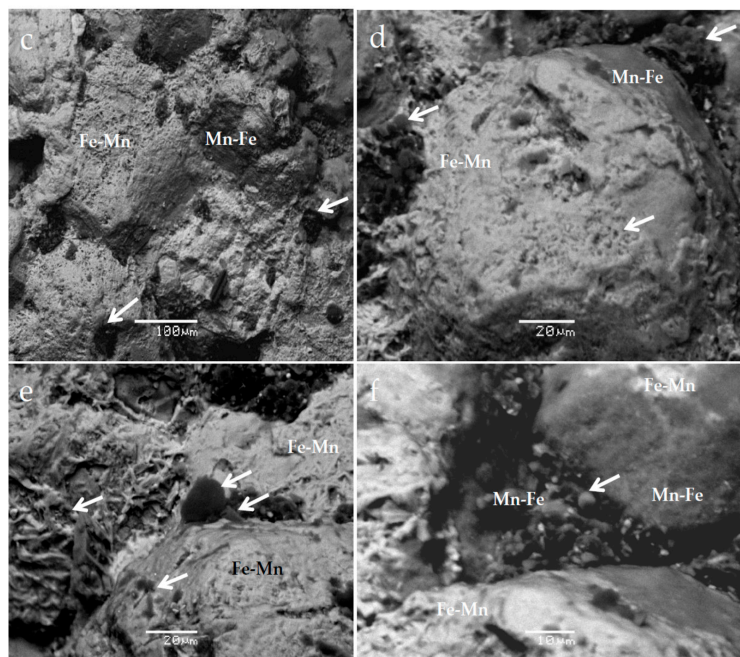


Figure 3. (a) Photograph of a Fe-Mn sample hosted in limestone, from the Legrena valley, Lavreotiki. The Fe-Mn phases appear as irregular, hard dark brown-black crust on the surface of carbonates. They are, in general, parallel to the shear plane of a thrust fault, suggesting a brecciated zone; Representative back scattered images from unpolished samples showing (b): Rounded fragments to spherical of Fe-Mn porous ore, cemented by dark brown-black Mn-Fe mineralization; (c–f): The Mn-Fe matrix hosting spherical isolated and aggregates of vestiges (white arrows) of varying size. A replacement of Fe-Mn hydroxides by Mn-Fe ones can be seen (e, f).

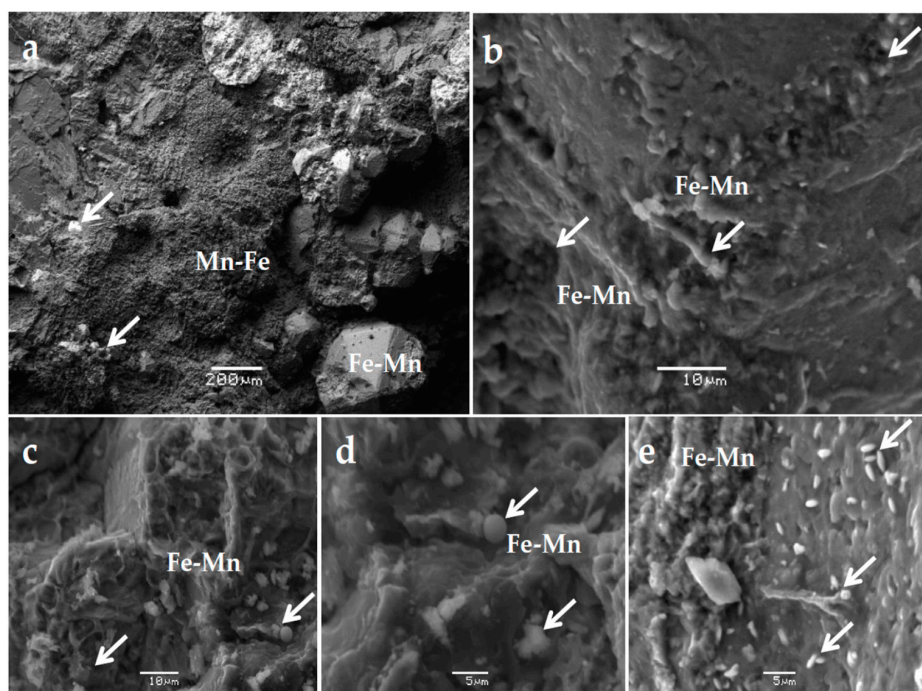


Figure 4. Representative secondary images of unpolished Fe-Mn hard dark brown-black crusts from the Legrena valley showing (a): Rounded fragments to spherical of Fe-Mn porous ore, cemented by dark brown-black Mn-Fe mineralization; (b–e): Ball-shaped Fe-Mn nodules, aggregates of vestiges and holdfasts (white arrows) are common.

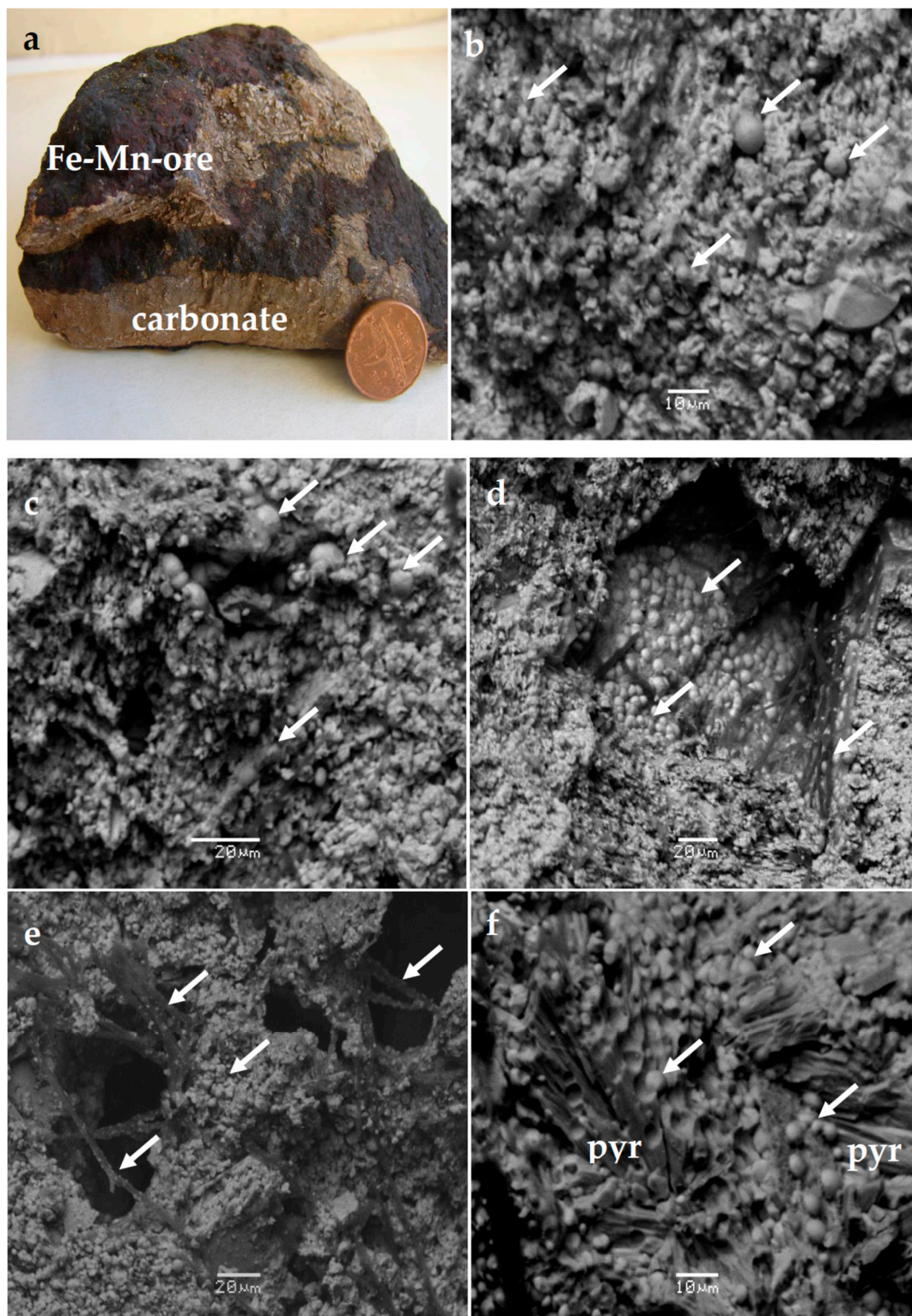


Figure 5. (a) Photograph of folded Fe-Mn ore sample hosted in limestone, from the Legrena valley, Lavreotiki. Back scattered images from unpolished samples showing (b–d): Consortium of bacteria fossils (white arrows) including abundant sphere or coccus (monococcus, diplococcus or packets) and filaments (d, e) within a matrix of goethite. Goethite coated spherical fossilized bacteria and/or removed mold spheroidals on pyrolusite crystals (pyr) is remarkable (f; see Table 2).

3. Materials and Methods

Bulk Fe-Mn mineralization samples of massive ore and of hard dark brown-black Fe-Mn crust were collected at the Legrena valley (Figures 1, 3a and 5a), from the brecciated and foliated zones of carbonate rocks, along their contact with the Kessariani schist.

Polished sections of all samples were examined using a reflected light microscope, a scanning electron microscope (SEM), and energy dispersive spectroscopy (EDS). The SEM-EDS semi-quantitative analyses were carried out at the Department of Geology and Geoenvironment, National and Kapodistrian University of Athens (NKUA), using a JEOL JSM 5600 SEM (JEOL, Tokyo, Japan), equipped with the ISIS 300 OXFORD automated energy dispersive X-ray analysis system. Analytical conditions were 20 kV accelerating voltage, 0.5 nA beam current, <2 µm beam diameter and 50 s count times. The following X-ray lines were used: AsLα, FeKα, NiKα, CoKα, CuKα, CrKα AlKα, TiKα, CaKα, SiKα, MnKα, MgKα, and ClKα. Pure metals standards were used for Mn, Cu, and Cr, and pyrite for S and Fe. Standard indium arsenide and 300 s counting time were used for As. In addition to well-polished sections, a few polished sections showing unpolished parts, revealing the presence of goethite micro-textures resembling bacterial cells, were coated by gold and analyzed, in order to identify traces of carbon and other components of organic material.

Major and trace elements in bulk samples were determined by inductively coupled plasma mass spectrometry (ICP-MS), at Bureau Veritas Labs, former ACME Laboratories Ltd., Vancouver, BC, Canada. The samples were dissolved using a strong multi-acid (HNO₃-HClO₄-HF) digestion and the residues dissolved in concentrated HCl.

X-ray powder diffraction (XRD) data were obtained at the Department of Geology and Geoenvironment, NKUA, using a Siemens Model 5005 X-ray diffractometer (Bruker AXS GmbH., Karlsruhe, Germany), CuKα radiation at 40 kV, 40 nA, 0.020 degrees/s step size and 1 s step time. The XRD patterns were evaluated using the EVA 10.0 program of the Siemens DIFFRAC (Bruker AXS GmbH., Karlsruhe, Germany) and the D5005 software package (NKUA).

4. Results

4.1. Mineralogical Characteristics

The XRD patterns of both massive Fe-Mn ore and hard dark brown-black Fe-Mn crusts (Figure 2), have showed mainly the presence of hematite, goethite, cryptomelane, pyrolusite and calcite (Table 1).

Table 1. Representative XRD analyses of Fe-Mn mineralized samples from the the Legrena valley, Lavrion (+: relative abundance of minerals).

| Mineral | Massive Fe-Mn Ore | Fe-Mn Crust |
|--------------|-------------------|-------------|
| Hematite | ++ | +++ |
| Goethite | ++ | ++ |
| Pyrolusite | ++ | ++ |
| Cryptomelane | + | ++ |
| Calcite | +++ | + |
| Feldspars | | + |
| Quartz | + | |

The above minerals identified by the XRD method are in good agreement with the minerals determined by SEM/EDS. The dominant Fe-oxide is hematite (Fe₂O₃). Calcite is almost pure, with low Mg and Fe contents. Iron-aluminum-silicates are abundant. An unusual feature in the studied Fe-Mn mineralization is the presence of spheroidal, bacteriomorphic Fe-hydroxides, composed of goethite. The high background and the broad peak shape on a XRD pattern (Figure 2), imply a low grade crystallinity of the major mineral phases (highly disordered solids).

Representative back scattered and secondary electron images from the dark brown to black Mn-Fe mineralization samples have revealed a consortium of bacteria fossils (white arrows), including abundant spheres or cocci and filaments of Fe-Mn hydroxides, within a fine-grained matrix (Figures 3–5).

Although the chemical composition of those fossilized bacteria was not determined exactly due to their very small size, they exhibit a wide chemical range (Table 2). Ball-shaped Fe-Mn nodules often show holes in the center (Figures 3d and 4b–d). SEM-EDS data of ball-shaped, with or without holes, and their holdfasts, has indicated a mixed composition (including Fe, Mn, Si, Al, As, Ti, P, Ca, K, Na and Cl) of fine-grained Mn-Fe-hydroxides with silicate minerals. Furthermore, EDS qualitative analyses on unpolished sections of those ore samples that were coated by gold, revealed the presence of carbon.

Table 2. Representative scanning electron microscope (SEM)-energy dispersive spectroscopy (EDS) analyses from the Fe-Mn-mineralization at the Legrena valley, Lavrion.

| Oxide wt % | Small Nodules (Figure 3) | | | | | | | | | | | |
|--------------------------------|--------------------------|------|--|------|------------------------------------|------|-------------------------------|------|------|---|--------|------|
| | Goethite (FeOOH) | | Hematite (Fe ₂ O ₃) | | Limonite FeO(OH)·nH ₂ O | | Figure 5c–f (Black-Spherical) | | | | Matrix | |
| SiO ₂ | 5.2 | 2.4 | 6.1 | 2.2 | 3.9 | n.d. | 22.1 | 25.4 | 25.1 | 3.6 | 6.2 | 40.7 |
| Al ₂ O ₃ | 3.9 | n.d. | 4.8 | n.d. | n.d. | 7.6 | 12.1 | 16.3 | 15.1 | 2.1 | 3.1 | 25.6 |
| Fe ₂ O ₃ | 73.8 | 85.1 | 74.8 | 96.8 | 92.6 | 59.2 | 39.8 | 34.8 | 24.3 | 9.7 | 37 | 19.4 |
| TiO ₂ | n.d. * | n.d. | n.d. | n.d. | n.d. | n.d. | 1.4 | 0.4 | 0.5 | n.d. | 0.4 | 0.5 |
| MnO | 0.6 | 0.9 | n.d. | n.d. | n.d. | 0.6 | 5.9 | n.d. | n.d. | n.d. | n.d. | n.d. |
| MgO | n.d. | n.d. | n.d. | 0.6 | 1.6 | n.d. | n.d. | n.d. | n.d. | n.d. | n.d. | 3.5 |
| CaO | n.d. | n.d. | n.d. | n.d. | 0.5 | n.d. | 0.4 | 2.5 | 6.9 | 1.1 | 1.4 | 0.5 |
| K ₂ O | n.d. | n.d. | n.d. | n.d. | n.d. | 0.4 | 3.4 | 1.2 | 2.3 | 9.8 | 4.5 | 2.1 |
| Na ₂ O | n.d. | n.d. | n.d. | n.d. | n.d. | n.d. | n.d. | 3.5 | 3.3 | 10.9 | 7.1 | n.d. |
| SO ₄ | n.d. | n.d. | n.d. | n.d. | 0.8 | 0.7 | 0.8 | 5.3 | 6.1 | 1.6 | n.d. | n.d. |
| As ₂ O ₃ | n.d. | n.d. | 2.8 | n.d. | n.d. | n.d. | 2.2 | 4.9 | 3.2 | 2.1 | 1.4 | n.d. |
| P ₂ O ₅ | n.d. | n.d. | n.d. | n.d. | 1.1 | n.d. | n.d. | 3.7 | 0.8 | 1.8 | n.d. | 1.3 |
| Cl | n.d. | n.d. | n.d. | n.d. | n.d. | n.d. | n.d. | n.d. | 1.4 | 8.6 | 4.1 | n.d. |
| Total | 83.5 | 88.4 | 88.5 | 99.6 | 101 | 68.5 | 88.1 | 98.0 | 89.0 | 42.7 | 62.0 | 93.6 |
| Oxide wt % | Figure 5b–d (Spherical) | | | | | | Figure 3 (Fillaments) | | | Figure 3f (Pyrolusite, MnO ₂) | | |
| SiO ₂ | 6.6 | 5.7 | 49.2 | 3.9 | 0.2 | 1.2 | 1.4 | 1.6 | 9.9 | 1.2 | n.d. | n.d. |
| Al ₂ O ₃ | 2.9 | 3.1 | 18.9 | 2.1 | n.d. | 0.5 | n.d. | n.d. | 6.1 | n.d. | n.d. | n.d. |
| Fe ₂ O ₃ | 15.2 | 6.5 | 8.3 | 72.5 | 76.8 | 74.6 | 76.3 | 77.9 | 8.9 | 87.6 | 95 | 1.3 |
| TiO ₂ | n.d. | n.d. | 0.8 | n.d. | n.d. | n.d. | n.d. | n.d. | n.d. | n.d. | n.d. | n.d. |
| MnO | 43.3 | 55 | 0.5 | 2.8 | 6.2 | 1.6 | 4.4 | 4.1 | 54.7 | 3.1 | 3.7 | 76.3 |
| MgO | 1.4 | 2.5 | 5.3 | 2.4 | n.d. | 0.9 | 1.3 | 0.6 | 4.2 | 0.9 | 0.5 | n.d. |
| CaO | n.d. | 1.5 | 1.5 | n.d. | n.d. | 1.1 | n.d. | 0.4 | 2.1 | 0.3 | n.d. | n.d. |
| K ₂ O | n.d. | 1.3 | 3.1 | n.d. | n.d. | 1.8 | n.d. | n.d. | 1.3 | 0.4 | n.d. | n.d. |
| Na ₂ O | 2.8 | 7.3 | n.d. | n.d. | n.d. | n.d. | n.d. | 1.5 | 7.1 | n.d. | n.d. | n.d. |
| SO ₄ | 0.9 | 1.9 | n.d. | n.d. | n.d. | 3.2 | n.d. | n.d. | 2.3 | 1.4 | n.d. | n.d. |
| As ₂ O ₃ | n.d. | n.d. | n.d. | n.d. | n.d. | n.d. | n.d. | n.d. | n.d. | n.d. | n.d. | n.d. |
| P ₂ O ₅ | n.d. | n.d. | 1.4 | n.d. | n.d. | 1.1 | n.d. | n.d. | 0.8 | n.d. | n.d. | n.d. |
| Cl | n.d. | n.d. | n.d. | n.d. | n.d. | n.d. | n.d. | n.d. | n.d. | n.d. | n.d. | n.d. |
| Total | 73.1 | 87.2 | 89.0 | 83.7 | 83.2 | 86.0 | 83.4 | 86.1 | 99.9 | 94.9 | 100.0 | 77.6 |

* n.d.: not detected.

4.2. Geochemical Characteristics

Whole-rock analyses (major and trace elements) of representative samples of massive Fe-Mn ore and hard dark brown-black Fe-Mn crust, hosted within brecciated and foliated zones of carbonate rocks from the Legrena valley, are presented in Table 3. Since hard dark brown-black Fe-Mn crust are of small thickness, the widest variation of Fe₂O₃ and CaO is obviously related to the proportion of the Fe-Mn ore and carbonates in the studied samples. Components of the mixed sulphides of the Lavrion mine, such as Pb, Zn and Cu, are lower in massive ore than in the thin hard crust, occurring along carbonate shear zones (Figures 3–5). Furthermore, the latter samples are characterized by slightly elevated As and Ba contents.

Table 3. Representative bulk analyses of Fe-Mn mineralized samples from the the Legrena valley, Lavrion.

| Element (ppm) | L.B1 | L.B2 | L.B.3 | L.B4 | Detection Limit |
|---------------|--------|--------|--------|--------|-----------------|
| Mo | | | | | 0.1 |
| Cu | 9.2 | 2.5 | 16 | 21 | 0.5 |
| Ni | 46 | 1.8 | 164 | 121 | 0.5 |
| Co | 21 | 9 | 17 | 12 | 1 |
| Pb | 9 | 100 | 6.6 | 3.5 | 0.5 |
| Zn | 7 | 197 | 23 | 12 | 5 |
| Cr | 1 | 3 | 1 | 1.7 | 1 |
| Mn | 1220 | 4270 | 6320 | 6700 | 5 |
| As | 130 | 77 | 16 | 10 | 5 |
| Sr | 200 | 17 | 20 | 16 | 5 |
| Cd | 0.2 | 0.5 | <0.5 | 0.8 | 0.5 |
| Sb | 0.7 | 1.8 | 13 | 6.5 | 0.5 |
| V | <2 | <2 | <2 | 2 | 10 |
| La | 5 | 6 | 7 | 3 | 0.5 |
| Ba | 22 | 238 | 36 | 18 | 5 |
| W | 70 | 60 | 86 | 45 | 0.5 |
| Zr | <0.5 | <0.5 | <0.5 | <0.5 | 0.5 |
| Y | 16 | 18 | 20 | 20 | 0.5 |
| % | | | | | |
| Fe | 8.29 | 3.28 | 53.4 | 48.4 | 0.01 |
| Al | <0.001 | 0.03 | 0.3 | 0.02 | 0.01 |
| Ti | <0.001 | <0.001 | <0.001 | <0.001 | 0.001 |
| Mg | 7.12 | 0.13 | 0.06 | 0.02 | 0.01 |
| Ca | 20.31 | 34.15 | 0.05 | 0.04 | 0.01 |
| P | 0.03 | 0.02 | 0.03 | 0.02 | 0.01 |
| Na | 0.01 | 0.02 | 0.01 | 0.005 | 0.01 |
| K | 0.01 | 0.01 | 0.16 | 0.03 | 0.01 |
| S | 0.05 | 0.06 | <0.05 | 0.09 | 0.05 |

5. Discussion

Recent studies have focused on hydrothermal systems in the South Aegean Volcanic Arc (SAVA), associated with Fe-Mn oxide/hydroxide ore deposits, including the region of Lavrion (Lavreotiki) [23–29]. The spatial heterogeneity of bacterial populations at a shallow-water hydrothermal vent near Milos Island (SAVA, Greece), has been largely influenced by photosynthesis. The water vents of Milos island are comparable to those reported in other shallow-water and deep-sea hydrothermal systems [29,30]. Also, fossilized iron bacteria provide evidence for anoxygenic photoferrotrophic deposition into banded iron rocks in shallow marine waters, associated with an Early Quaternary hydrothermal vent field on Milos Island, Greece [31].

The carbonate hosted replacement mixed sulphide ore (B.P.G) of sphalerite, galena and pyrite at Lavrion, are spatially related to the late Miocene detachment faults, shear zones within carbonates and contacts, between marbles and the intercalated metaclastic subunit, while the supergene mineral assemblages, occupy secondary open spaces and occur as replacement pods within marble [1–3,5–7].

Although, the amount of Si, Al, As, Ti, P, Ca, K, Na and Cl, in the films covering bacteriomorphic Fe-Mn oxides/hydroxides at the Legrena valley, exhibit variable contents and the SEM/EDS analyses and may be semi-quantitative (Table 2), they provide some evidence for a similarity between the spherical-shaped filaments and their holdfast material. Moreover, compared to the common massive Fe-Mn ore, they differ in terms of: (a) the extensive occurrence of bacteriomorphic Fe-oxides/hydroxides and their micro-textures (Figures 3–5); and (b) certain minor elements (Tables 2 and 3). The significant Na and Cl contents, in some spherical bacteriomorphic Fe-Mn-hydroxides at the Legrena valley (Table 2), seem to be a salient feature. Halophilic bacteria are usually related

to hypersaline regions, containing 20–30% NaCl, such as the Dead Sea and the Great Salt Lake [32]. In addition to the important control by the physico-chemical conditions, redox potential, solubility and supersaturation [33,34], the formation of Fe-Mn oxides/hydroxides may involve reactions catalyzed by microorganisms.

5.1. The Potential Role of Microorganisms in the Redox Reactions

Assuming that the primary interaction between organic and inorganic system may be transformed, and/or lose their primary characteristics, the observed features of the Fe-Mn ores are complicated, and therefore the investigation of Mn-Fe mineralization requires a multidisciplinary approach. However, it is clear that the microorganism activity may cause a change of the original characteristics of the inorganic system. The enrichment of variable valence elements and common components of microorganism, such as of Si, Al, As, Ti, P, Ca, K, Na and Cl (Tables 2 and 3), may be characteristic of such bacterial activity and point to the role of microorganisms, in precipitating elements from solution/fluids.

Bio-minerals may be formed as a by-product of metabolic activity, or organic matter-metal interaction [35], and may differ distinctly from the inorganically formed equivalents in shape, size, isotopic, and trace element composition [36–41]. Negatively charged surfaces of bacteria cells offer extensive surfaces for biosorption of metals, where elements with a higher positive charge are preferentially adsorbed [37,42]. Both metabolic activity and bio-mineral precipitation by organisms may play an important role in trace element co-precipitation [37,38,42,43]. A consortium of microorganisms of varying morphological forms (filament-like and spherical to lenticular of an average size 2 μm), producing enzymes, has been considered to be a powerful catalyst that catalyze the redox reactions in bauxites, allow faster rates of metal extraction and provide alternative pathways for the beneficiation of bauxite ore [44,45]. In general, Mn-Fe oxides/hydroxides in the environment appear to be comparable to those produced in laboratory cultures, specifically poorly crystalline minerals [46,47]. The biomineralization of Fe-Mn hydroxides and silicates on capsuled bacterial cell walls has been described to be grown in freshwater microorganism mats [46]. Using SEM and Transmission Electron Microscopy (TEM) for the investigation of microorganism mats, it has been concluded that well-developed holdfasts on *Leptothrix discophora* bacterial cells were, mainly, associated with poorly crystalline layer silicates and Fe-Mn hydroxides [46]. More specifically, abundant micro-colonies of rod- and coccus-shaped bacteria with layer-silicate thin films, were developed in three weeks in freshwater, having a range in pH between 6.3 and 7.8, temperature 12 °C to 20 °C and Eh -24 to $+200$ mV [46]. Furthermore, a thermodynamic approach to biomineralization suggests possible ways, in which organisms can control the formed phases and their morphology [34]. It has been suggested that the oxyhydroxide ferrihydrite is metastable, with respect to goethite, as nanoparticulates under typical surface conditions, has high specific surface area and significant reactivity toward the sorption of elements [34].

5.2. Multistage Fe-Mn Mineralization

The genesis of the studied Fe-Mn mineralization through Attica seems to be the result of multistage supergene processes superimposed over initial hydrothermal stages [1,2,5–7]. The occurrence of the thin, hard, dark, brown to black Fe-Mn crusts at the Legrena valley area, located within brecciated and foliated zones of carbonates, may reflect remobilization and precipitation of metals along open space surfaces on karstified carbonates, during a subsequent stage of their initial precipitation at the Legrena valley. Goethite becomes thermodynamically stable, relative to hematite and water at particle sizes of 60 nm (assuming spherical particles), while at high surface areas, ferrihydrite is thermodynamically very competitive with the other iron oxides. The particle size exerts major control over the relative stability and formation of hematite and goethite. The hematite-goethite equilibrium may also be shifted, by variations in temperature and water activity. Despite the fact that the direct transformation of hematite to goethite, or goethite to hematite, is uncertain in nature, the water

adsorption experiments have shown that hydrated hematite surfaces behave thermodynamically like the surfaces of goethite, and therefore transformation, in either direction, is possible [34]. Hence, the presence of Fe-Mn oxides/hydroxides as rounded fragments, resembling small nodules of varying size, may be the result of variations in the ratio of the circulated fluids and the reacted rocks, suggesting that it was favorable to cause their fragmentation (relatively dry conditions). The presence of Mn-Fe oxides/hydroxides in the matrix of the above rounded fragments is consistent with the higher solubility of manganese compared to iron in the circulated fluids [46–48]. Furthermore, the occurrence of Mn-Fe oxide/hydroxides as matrix between high-Fe rounded fragments and the stability of large idiomorphic crystals of pyrolusite (Figure 3f) required an alkaline environment ($\text{pH} > 7$). This is consistent with experimental data, indicating that at pH values higher than 8 (Eh-independent), Mn precipitation is enhanced [46]. Moreover, in the presence of calcium, a biooxide is produced having somewhat higher crystallinity [47].

6. Conclusions

The presented geological, mineralogical and geochemical data on Fe-Mn-mineralization from the Legrena valley, Lavrion, lead to the following conclusions:

- The occurrence of abundant bacteriomorphic Fe-Mn-oxides/hydroxides on Fe-Mn-mineralization from the Legrena valley indicates the catalytic role of microorganisms to the redox reactions during ore formation.
- The presence of microorganisms in Fe-Mn-hydroxides, combined with their chemical features (Na, Cl, K, P, S, Ca, and As), in particular the relatively high Na and Cl contents, may point to a saline environment.
- The relatively high background and broad peak shape in the X-ray powder diffraction (XRD) patterns of Fe-Mn samples suggest a low grade crystallinity of the major mineral phases.

Acknowledgments: The National and Kapodistrian University of Athens (NKUA) is greatly acknowledged for the financial support (Grant No. KE_11078) of this work. Vasilis Skounakis is thanked for his assistance with the SEM-EDS analyses. Many thanks are expressed to the anonymous reviewers for their constructive criticism and suggestions to an earlier draft of the manuscript.

Author Contributions: C.V. collected the samples, provided the field information and performed all types of analyses. Both authors (C.V. and M.E.-E.) contributed to the elaboration and interpretation of the data and to the final revision of the manuscript.

Conflicts of Interest: The authors declare no conflict of interest.

References

1. Marinos, G.P.; Petrascheck, W.E. Laurium. *Geol. Geophys. Res.* **1956**, *4*, 1–247.
2. Skarpelis, N. The Lavrion deposit (SE Attica, Greece): Geology, mineralogy and minor elements chemistry. *Neues Jahrb. Mineral. Abh.* **2007**, *183*, 227–249. [[CrossRef](#)]
3. Voudouris, P.; Economou-Eliopoulos, M. Mineralogy and chemistry of Cu-rich ores from the Kamariza carbonate hosted deposit (Lavrion), Greece. In *Mineral Exploration and Sustainable Development*; Eliopoulos, D., Ed.; Millpress: Rotterdam, The Netherlands, 2003; pp. 499–502.
4. Bonsall, T.A.; Spry, P.G.; Voudouris, P.; St Seymour, K.; Tombros, S.; Melfos, V. Fluid inclusion and stable isotope characteristics of carbonate replacement Pb-Zn-Ag deposits in the Lavrion district, Greece. In *Mineral Exploration and Research: Digging Deeper*; Irish Association for Economic Geology: Dublin, Ireland, 2007; pp. 283–286.
5. Skarpelis, N.; Ardyraki, A. Geology and origin of supergene ore at the Lavrion Pb-Ag-Zn deposit, Attica, Greece. *Resour. Geol.* **2008**, *59*, 1–14. [[CrossRef](#)]
6. Voudouris, P.; Melfos, V.; Spry, P.; Bonsall, T.; Tarkian, M.; Economou-Eliopoulos, M. Mineralogical and fluid inclusion constraints on the evolution of the Plaka intrusion-related ore system, Lavrion, Greece. *Miner. Petrol.* **2008**, *93*, 79–110. [[CrossRef](#)]

7. Berger, A.; Schneider, D.; Grasmann, B.; Stockli, D. Footwall mineralization during Late Miocene extension along the West Cycladic Detachment System, Lavrion, Greece. *Terra Nova* **2012**, *25*, 181–191. [[CrossRef](#)]
8. Dando, P.; Aliani, S.; Arab, H.; Bianchi, C.; Brehmer, M.; Cocito, S.; Fowlers, S.W.; Gundersen, J.; Hooper, L.E.; Kölblh, R.; et al. Hydrothermal studies in the Aegean Sea. *Phys. Chem. Earth B Hydrol. Oceans Atmos.* **2000**, *25*, 1–8. [[CrossRef](#)]
9. Kampouroglou, E.; Economou-Eliopoulos, M. Natural contamination by as and heavy metals in soil, their bio-accumulation and potential sources: The case of a travertine limestone quarry, Greece. *Cent. Eur. J. Geosci.* **2013**, *5*, 174–188. [[CrossRef](#)]
10. Kampouroglou, E.; Economou-Eliopoulos, M. Assessment of the environmental impact by as and heavy metals in lacustrine travertine limestone and soil in Attica, Greece: Mapping of potentially contaminated sites. *Catena* **2016**, *139*, 137–166. [[CrossRef](#)]
11. Stouraiti, C.; Lekkas, S.; Lozios, S.; Kanellopoulos, C. Iron-oxide mineralization of Sesi, Koropi (S. Hymittos, Greece): Mineralization within a detachment zone. *Bull. Geol. Soc. Greece* **2016**, *50*, 2025–2036. [[CrossRef](#)]
12. Conofagos, K. *The Ancient Laurium and the Greek Technique for Silver Production*; Ekdotiki Athinon: Athens, Greece, 1980; 458p.
13. Papanikolaou, D.J.; Syskakis, D. Geometry of acid intrusives in Plaka, Laurium and relation between magmatism and deformation. *Bull. Geol. Soc. Greece* **1991**, *25*, 355–368.
14. Photiades, A.; Carras, N. Stratigraphy and geological structure of the Lavrion area (Attica, Greece). *Bull. Geol. Soc. Greece* **2001**, *34*, 103–109.
15. Marakis, G. Remarks on the age of sulfide mineralization in Cyclades area. *Ann. Geol. Pays. Hell.* **1968**, *19*, 695–700.
16. Altherr, R.; Kreuzer, H.; Wendt, I.; Lenz, H.; Wagner, G.A.; Keller, J.; Harre, W.; Hohndorf, A. A late Oligocene/early Miocene high temperature belt in the Attic-Cycladic crystalline complex (SE Pelagonian, Greece). *Geol. Jahrb.* **1982**, *E23*, 97–164.
17. Pe-Piper, G.; Piper, D. *The Igneous Rocks of Greece: Anatomy of an Orogen*, 1st ed.; Beiträge zur Regionalen Geologie der Erde: Stuttgart, Germany, 2002; 588p, ISBN 978-3-443-11030-7.
18. Tsikouras, B.; Karipi, S.; Grammatikopoulos, T.A.; Hatzipanagiotou, K. Listwaenite evolution in the ophiolite mélange of Iti mountain (Continental Central Greece). *Eur. J. Mineral.* **2006**, *18*, 243–255. [[CrossRef](#)]
19. Skarpelis, N.; Tsikouris, B.; Pe-Piper, G. The Miocene igneous rocks in the Basal Unit of Lavrion (SE Attica, Greece): Petrology and geodynamic implications. *Geol. Mag.* **2007**, *145*, 1–15. [[CrossRef](#)]
20. Skarpelis, N. Geodynamics and evolution of the Miocene mineralization in the Cycladic-Pelagonian Belt, Hellenides. *Bull. Geol. Soc. Greece* **2002**, *34*, 2191–2209.
21. Economou, M.; Skounakis, S.; Papathanasiou, C. Magnetite deposits of skarn type from the Plaka area of Laurium, Greece. *Chem. Erde* **1981**, *40*, 241–252.
22. Gelaude, P.; van Kalmthout, P.; Rewitzer, C. *Laurion: The Minerals in the Ancient Slags*; Janssen Print: Nijmegen, The Netherlands, 1996; 195p.
23. Dando, P.R.; Thomm, M.; Arab, H.; Brehmer, M.; Hooper, L.; Jochimsen, B.; Schlesner, H.; Stohr, R.; Miquel, J.-C.; Fowler, S. Microbiology of shallow hydrothermal sites off Palaeochori Bay, Milos (Hellenic Volcanic Arc). *Cah. Biol. Mar.* **1999**, *39*, 369–372.
24. Hein, J.R.; Stamatakis, G.M.; Dowling, S.J. Trace metal-rich Quaternary hydrothermal manganese oxide and barite deposit, Milos Island, Greece. *Appl. Earth Sci.* **2000**, *109*, 67–76. [[CrossRef](#)]
25. Hein, J.R.; Schulz, M.S.; Dunham, R.E.; Stern, R.J.; Bloomer, S.H. Diffuse flow hydrothermal manganese mineralization along the active Mariana and southern Izu-Bonin arc system, western Pacific. *J. Geophys. Res.* **2008**, *113*, B08S14. [[CrossRef](#)]
26. Kiliadis, S.P.; Naden, J.; Cheliotis, I.; Shepherd, T.J.; Constandinidou, H.; Crossing, J.; Simos, I. Epithermal gold mineralization in the active Aegean volcanic arc: The Profitis Ilias deposit, Milos Island, Greece. *Miner. Deposita* **2001**, *36*, 32–44. [[CrossRef](#)]
27. Alfieris, D.; Voudouris, P.; Spry, P.G. Shallow submarine epithermal Pb-Zn-Cu-Au-Ag-Te mineralization on western Milos Island, Aegean Volcanic Arc, Greece: Mineralogical, geological and geochemical constraints. *Ore Geol. Rev.* **2013**, *53*, 159–180. [[CrossRef](#)]
28. Petersen, S.; Monecke, T.; Westhues, A.; Hannington, M.D.; Gemmel, J.B.; Sharpe, R.; Peters, M.; Strauss, H.; Lackschewitz, K.; Augustin, N.; et al. Drilling shallow-water massive sulfides at the Palinuro Volcanic Complex, Aeolian Island Arc, Italy. *Econ. Geol.* **2014**, *109*, 2129–2158. [[CrossRef](#)]

29. Giovannelli, D.; d' Errico, G.; Manini, E.; Yakimov, M.; Vetriani, C. Diversity and phylogenetic analyses of bacteria from a shallow-water hydrothermal vent in Milos island (Greece). *Front. Microbiol.* **2013**, *4*, 184. [[CrossRef](#)] [[PubMed](#)]
30. Sievert, S.M.; Brinkhoff, T.; Muyzer, G.; Ziebis, W.; Kuever, J. Spatial heterogeneity of bacterial populations along an environmental gradient at a shallow submarine hydrothermal vent near Milos Island (Greece). *Appl. Environ. Microbiol.* **1999**, *65*, 3834–3842. [[PubMed](#)]
31. Chi Fru, E.; Ivarsson, M.; Kiliass, S.P.; Bengtson, S.; Belivanova, V.; Marone, F.; Fortin, D.; Broman, C.; Stampanoni, M. Fossilized iron bacteria reveal a pathway to the biological origin of banded iron formation. *Nat. Commun.* **2013**, *4*, 2050. [[CrossRef](#)] [[PubMed](#)]
32. Post, F.J. The microbial ecology of the Great Salt Lake. *Microb. Ecol.* **1977**, *3*, 143–165. [[CrossRef](#)] [[PubMed](#)]
33. Ehrlich, L.E. *Geomicrobiology*, 4th ed.; Marcel Decker: New York, NY, USA, 2002; 768p, ISBN 0-8247-0764-8.
34. Navrotsky, A.; Mazeina, L.; Majzslan, J. Size driven structural and thermodynamic complexity in iron oxides. *Science* **2008**, *319*, 1635–1638. [[CrossRef](#)] [[PubMed](#)]
35. Lowenstam, A.H.; Weiner, S. *On Biomineralization*; Oxford University Press: New York, NY, USA, 1989; 336p, ISBN 0-19-504977-2.
36. Bazylinski, D.A.; Schübbe, S. Controlled biomineralization by and applications of magnetotactic bacteria. *Adv. Appl. Microbiol.* **2007**, *62*, 21–62. [[CrossRef](#)] [[PubMed](#)]
37. Haferburg, G.; Kothe, E. Microbes and metals: Interactions in the environment. *J. Basic Microbiol.* **2007**, *47*, 453–467. [[CrossRef](#)] [[PubMed](#)]
38. Heim, C. An Integrated Approach to the Study of Biosignatures in Mineralizing Biofilms and Microbial Mats. Ph.D. Thesis, Georg-August-Universität Göttingen, Göttingen, Germany, 2010.
39. Konhauser, K. Bacterial iron biomineralization in nature. *FEMS Microbiol. Rev.* **1997**, *20*, 315–326. [[CrossRef](#)]
40. Pósfai, M.; Buseck, P.R.; Bazylinski, D.A.; Frankel, R.B. Reaction sequence of iron sulfide minerals in bacteria and their use as biomarkers. *Science* **1998**, *280*, 880–883. [[PubMed](#)]
41. Pósfai, M.; Buseck, P.R.; Bazylinski, D.A.; Frankel, R.B. Iron sulfides from magnetotactic bacteria: Structure, compositions, and phase transitions. *Am. Mineral.* **1998**, *83*, 1469–1481. [[CrossRef](#)]
42. Texier, A.C.; Andres, Y.; le Cloirec, P. Selective biosorption of lanthanide (La, Eu, Yb) ions by *Pseudomonas aeruginosa*. *Environ. Sci. Technol.* **1999**, *33*, 489–495. [[CrossRef](#)]
43. Ferris, G.F.; Hallberg, O.R.; Lyvén, B.; Pedersen, K. Retention of strontium, cesium, lead and uranium by bacterial iron oxides from a subterranean environment. *Appl. Geochem.* **2000**, *15*, 1035–1042. [[CrossRef](#)]
44. Laskou, M.; Economou-Eliopoulos, M. Bio-mineralization and potential biogeochemical processes in bauxite deposits: Genetic and ore quality significance. *Miner. Petrol.* **2013**, *107*, 471. [[CrossRef](#)]
45. Laskou, M.; Economou-Eliopoulos, M. The role of microorganisms on the mineralogical and geochemical characteristics of the Parnassos-Ghiona bauxite deposits, Greece. *J. Geochem. Explor.* **2007**, *93*, 67–77. [[CrossRef](#)]
46. Tazaki, K. Biomineralization of layer silicates and hydrated Fe/Mn oxides in microbial mats: An electron microscopical study. *Clays Clay Miner.* **1997**, *45*, 203–212. [[CrossRef](#)]
47. Tebo, B.M.; Bargar, J.R.; Clement, B.; Dick, G.; Murray, K.J.; Parker, D.; Verity, R.; Webb, S. Manganese biooxides: Properties and mechanisms of formation. *Annu. Rev. Earth Planet. Sci.* **2004**, *32*, 287–328. [[CrossRef](#)]
48. Brookins, D.G. *Eh-pH Diagrams for Geochemistry*; Springer: Berlin, Germany, 1988; 176p.

